ELSEVIER

Computational Materials Science 29 (2004) 165–178

COMPUTATIONAL MATERIALS SCIENCE

www.elsevier.com/locate/commatsci

Bulk properties and electronic structure of $SrTiO_3$, $BaTiO_3$, $PbTiO_3$ perovskites: an ab initio HF/DFT study

S. Piskunov [a,*], E. Heifets [b], R.I. Eglitis [a], G. Borstel [a]

[a] *Fachbereich Physik, Universität Osnabrück, D-49069 Osnabrück, Germany*
[b] *California Institute of Technology, MS 139-74, Pasadena, CA 91125, USA*

Received 13 March 2003; received in revised form 2 June 2003; accepted 12 August 2003

Abstract

The results of detailed calculations for bulk properties and the electronic structure of the cubic phase of $SrTiO_3$ (STO), $BaTiO_3$ (BTO), and $PbTiO_3$ (PTO) perovskite crystals with detailed optimization of basis set (BS) are discussed. These are obtained using ab initio Hartree–Fock (HF) and density functional theory (DFT) with Hay–Wadt pseudopotentionals based on localized, Gaussian-type BS. A number of different exchange–correlation functionals including hybrid (B3PW and B3LYP) exchange techniques are used. Results, obtained for seven methods, are compared with previous quantum mechanical (QM) calculations and available experimental data. Especially good agreement with the experimental data has been achieved for hybrid functionals. With the polarization orbitals added to the BS of oxygen atom, the calculated optical band gaps are 3.57, 3.42 and 2.87 eV for STO, BTO and PTO respectively, in very good agreement with experimental data.

PACS: 61.20.Ja; 62.20.Dc; 71.20.−b; 71.25.Tn
Keywords: $SrTiO_3$; $BaTiO_3$; $PbTiO_3$; Elastic properties; Electronic properties; Gaussian basis sets; Ab initio calculations

1. Introduction

ABO_3-type perovskite crystals are important for numerous technological applications in electro-optics, waveguides, laser frequency doubling, high capacity computer memory cells, etc. [1–4]. The perovskite-type materials have been under intensive investigation at least for half a century, but, from theoretical point of view, a proper description of their electronic properties is still an area of active research. The electronic structure of perovskites has been recently calculated from first principles and published by several research groups. One of the first theoretical investigations of the ferroelectric transitions in BTO and PTO perovskite crystals have been performed by Cohen and Krakauer in the beginning of 90s [5–7]. Authors used the all-electron full-potential linearized augmented-plane-wave method within the local density approximation (LDA). In 1994 the systematic study of structural and dynamical

* Corresponding author. Tel.: +49-541-969-2620; fax: +49-541-969-2351.
E-mail address: spiskuno@uos.de (S. Piskunov).

0927-0256/$ - see front matter © 2003 Elsevier B.V. All rights reserved.
doi:10.1016/j.commatsci.2003.08.036

properties for eight various perovskites has been published by King-Smith and Vanderbilt [8]. They used the ultrasoft-pseudopotential method and the LDA. A few years later Tinte and Stachiotti [9] reported the results of local spin density approximation and Perdew–Burke–Erzernhof generelaized gradient approximation (GGA) calculations for above-mentioned properties of four perovskite oxides. Most recently, Cora and Catlow examined the electronic structure of a wide range of perovskites using ab initio HF method [10]. Also, the detailed description of the atomic and electronic properties of PTO can be found in studies performed by Ghosez, Waghmare and co-workers [11,12], and Cappellini et al. who applied a perturbative approximation, based on a set of self-consistent equations for the one-electron Green's function involving a screened potential, to the calculations of ground-state properties of STO and related binary ionic oxides, SrO and MgO [13]. All these studies show the considerable progress in calculations of various perovskite properties and understanding the origin of ferroelectricity. However, the previously calculated optical band gaps and lattice structure parameters are in disagreement with the relevant experimental results. Indeed, band gap calculated using the Kohn–Sham (KS) Hamiltonian usually strongly underestimates the experimental results, but, on the other hand, the HF overestimates the gap severely. Therefore, applying so-called *hybrid* exchange–correlation techniques could improve the accuracy of the band gap calculation.

The elastic constants C_{ij} play an important role in the physics of materials as they characterize the behavior of the crystal in the field of external forces, e.g. on the substrate. C_{ij} can be easily determined from the first principles calculations done in the direct computation. Nevertheless, only a few of the mentioned ab initio studies [8,12] discuss calculations of the elastic constants for perovskite crystals. In this paper, we present a detail comparison of calculated elastic constants, using different approximation, with existing theoretical and experimental data.

In order to continue our previous studies of perovskite surfaces [14–16], as well as to extend our investigations on perovskite solid solutions, multi-layer structures, interfaces of perovskites with other materials, and defects in perovskites, we performed a detailed comparative study based on a number of different QM techniques including hybrid exchange–correlation functionals. This comparison allows us to select the exchange–correlation functional, which describes well the lattice structure of perovskite crystals, their elastic properties, and the optical band gap.

In present simulations we employ effective core potentials (ECPs). This approximation allows one to replace the chemically inert core electrons with the effective potentials and hence, to focus on more significant calculations of the valence electron states, and thus to save significant amount of computational time.

In order to perform first-principles HF and DFT calculations we used the CRYSTAL computer code. This code has been under continuous development for about quarter of a century [17–25]. CRYSTAL is the periodic-structure computer program that uses the functions localized at atoms as the basis for expansion of the crystalline orbitals. This approach is usually called linear combination of atomic orbitals (LCAO) technique. The great advantage of this code is the ability to calculate the electronic structure of materials within both HF and KS Hamiltonians, or various hybrid approximations using the identical BS and other computational parameters. However, in order to employ this code, it is necessary to optimize BSs, which would be suitable for the electronic structure computations of crystals.

In this paper, we study three important perovskite crystals: STO, BTO, and PTO. BSs for oxygen, titanium, strontium, barium and lead have been published earlier in several studies (see Ref. [26] and references therein) and are widely used. Our previous studies [14–16] show that in order to improve description of the perovskite crystal properties, d-orbitals should be added to the oxygen BS. Simultaneously, because we employ the ECP instead of the explicit core electrons on titanium, we also have to construct and to optimize a new BS for Ti. Also, we have to build up and optimize consistent BSs for other cations included in our simulations. Previously, we used ECPs only to replace the Sr and Ba cores in STO and BTO.

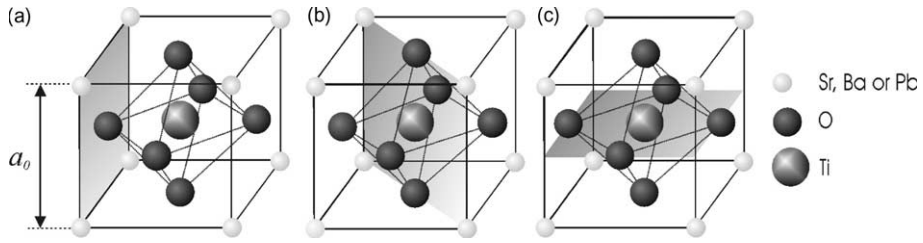

Fig. 1. Structural units of the cubic ABO_3 perovskite crystals cross-sectioned by three different planes (shaded): (a) the (1 0 0) surface AO termination, (b) the (1 1 0) surface, (c) the (0 0 1) surface with TiO_2 termination. The length a_0 is the lattice constant. The axes {1 0 0}, {0 1 0}, {0 0 1} begin at Sr atom and coincide with the edges of a cubic unit cell.

We have chosen perovskite crystals of a very simple, cubic Pm3m symmetry, in order to keep all computational conditions simple and identical. In fact, STO has a simple cubic structure above −168 °C, whereas BTO and PTO have a cubic symmetry above 130 and 490 °C, respectively. The well-known structure of a cubic perovskite is schematically displayed in Fig. 1. In this structure oxygen atoms, located in the face-center positions of a cubic unit cell, form a perfect octahedron with the titanium atom in its center, and strontium, barium or lead atoms lying outside the oxygen octahedron, in corners of a cube, the a_0 is the cube lattice constant. We are going to address properties of these perovskites in different phases in future studies.

Unique options provided by the CRYSTAL code allowed us to perform a consistent comparison between HF and DFT descriptions of the atomic and electronic properties of bulk perovskite crystals, including performance of the hybrid functionals.

The paper is organized as follows: in Section 2 we present the computational parameters including the BS description and methodology. In Section 3 we discuss a wide range of basic properties of cubic perovskite crystals (optimized lattice constants a_0, elastic constants C_{ij}, bulk modulus B, Mulliken population analysis, charge density, density of electronic states and the band structure). Our conclusions are summarized in Section 4.

2. Computational details

The Hay–Wadt "small-core" ECPs [27–29] have been adopted for Ti, Sr, and Ba atoms, and the "large-core" version of Hay–Wadt ECP for Pb atoms [27–29]. The 'small-core' ECPs replace only inner core orbitals, but orbitals for outer core electrons as well as for valence electrons are calculated self-consistently. Still, we use the full electron BS for the light oxygen atoms, whereas their outermost exponents were optimized. The BSs have been constructed and optimized in the following forms: O—8-411(1d)G, Ti—411(311d)G, Sr and Ba—311(1d)G, and Pb—211(1d) where the numbers refer to the level of contraction. In a comparison with the BSs [26], used in our previous studies [14–16], we added the polarization d-function on O, replaced the inner core orbitals of Ti by "small-core" Hay–Wadt ECP, and consistently used the two most diffuse s and p Gaussians as the separate basis functions on Ti, Ba, Sr, Pb.

In the LCAO computational schemes for crystals, each crystalline orbital is presented as a linear combination of the Bloch functions:

$$\phi_\mu(\mathbf{r};\mathbf{k}) = \sum_{\mathbf{g}} e^{i\mathbf{k}\mathbf{g}} \phi_\mu(\mathbf{r};\mathbf{g}). \quad (1)$$

The atom-centered basis functions $\phi_\mu(\mathbf{r};\mathbf{g})$ are expanded into a linear combination of individually normalized atom-centered Gaussian-type functions (GTF) with the fixed coefficients d_j and exponents α_j:

$$\phi_\mu(\mathbf{r};\mathbf{g}) = \sum_{j}^{n_G} d_{\mu j} G(\alpha_j;\mathbf{r}-\mathbf{A}_j-\mathbf{g}). \quad (2)$$

Here $\mathbf{g}$ is the lattice vector and $\mathbf{A}_j$ describes position of an atom inside the unit cell. A choice of the proper Gaussian BS should lead to the more accurate results. In principle, the quality of BS can

be improved by use of the additional functions and optimization of their exponents, for example, in a bulk crystal. On the other hand, it is necessary to avoid the overcompleteness of the BS, which leads to a linear dependence between basis functions on different atoms.

The basis set optimization procedure has been divided into several stages. In the first stage, the optimization of Gaussian exponents and contraction coefficients have been done through the energy minimization of the free-ion state of metal atoms (Ti^{4+}, Sr^{2+}, Ba^{2+}, Pb^{2+}), using the small computer code that implements conjugated gradients optimization [30] with a numerical computation of derivatives. In the second stage, using the same optimization code, we optimized the outer Gaussian exponents in bulk crystals through the minimization of the total energy per unit cell. This brings the BS into its final shape. The only exception is BS of an oxygen atom taken from Ref. [26]. The optimization of the outermost diffused exponents of oxygen atoms ($\alpha_{sp} = 0.5$ and 0.191 $bohr^{-2}$) in STO crystal leads to 0.452 and 0.1679, respectively. The oxygen d polarization orbital ($\alpha_d = 0.451$ $bohr^{-2}$) has been also added, which provides the flexibility to BS and reflects the oxygen additional polarizability in the crystalline environment. The same BS for oxygen was then employed for STO, BTO, and PTO. Final BSs obtained for metal ions are presented in Table 1. Thus, the Gaussian BSs have been successfully generated for all three perovskite oxides composed

Table 1
The exponents ($bohr^{-2}$) and contraction coefficients of individually normalized Gaussian-type basis functions

	Shell	Exponents	Coefficients		
			s	p	d
Ti	3sp	16.6627995	0.00528827652	−0.00247236521	
		3.82352098	0.348881629	−0.490787025	
		3.76734787	0.2	0.5	
		1.33437747	−0.846874184	0.047543445	
	4sp	0.7725692	1.0	1.0	
	5sp	0.4369296	1.0	1.0	
	3d	21.429541			0.0880789808
		6.08722431			0.417373956
		2.07945196			1.0
	4d	0.8310327			1.0
	5d	0.3562744			1.0
Sr	4sp	16.7295003	−0.0408649838	0.00642885488	
		2.23218348	1.0	1.0	
		1.98458795	9.26146754	−0.963768104	
	5sp	0.6537827	1.0	1.0	
	6sp	0.2609586	1.0	1.0	
	4d	0.4699451			1.0
Ba	5sp	8.55243254	0.00444607339	0.0108828307	
		2.113983	−0.760825674	−0.598137631	
		1.87184187	1.0	1.0	
	6sp	0.5087498	1.0	1.0	
	7sp	0.204084	1.0	1.0	
	5d	0.3319258			1.0
Pb	6sp	1.335104	−0.1448789	−0.1070612	
		0.7516086	1.0	1.0	
	7sp	0.5536686	1.0	1.0	
	8sp	0.1420315	1.0	1.0	
	6d	0.1933887			1.0

All atoms are described using the Hay–Wadt small core pseudopotentials [27–29].

of 18 atomic orbitals for O, 27 for Ti and 17 for Sr, Ba and Pb.

Using our newly generated BS, we have calculated the total energies and the electronic structures for all three crystals by means of several, quite different methods: "pure" HF and various DFT calculations, including hybrid functionals by Becke [39]. In our DFT computations, we used LDA with the Dirac–Slater exchange [31] and the Vosko–Wilk–Nusair correlation [32] energy functionals and a set of GGA exchange and correlation functionals as suggested by Perdew and Wang (PWGGA) [33–35], by Perdew, Burke and Ernzerhof (PBE) [36], and lastly by the Becke exchange potential [37] combined with the correlation potential by Lee, Yang and Parr (BLYP) [38]. We also performed calculations using the hybrid functionals [39] mixing the Fock exchange and Becke's gradient corrected exchange functional. We employed two versions of the gradient corrected correlation potentials together with hybrid exchange potentials: by Lee, Yang and Parr (B3LYP) or by Perdew and Wang (B3PW). For the DFT calculations, we expanded the exchange and correlation potentials in the auxiliary Gaussian BS (AUX) [18], whose minimum and maximum exponents are presented in Table 2. The reciprocal space integration was performed by a sampling the Brillouin zone with the $8 \times 8 \times 8$ Pack–Monkhorst net [40] which provides the balanced summation in the direct and reciprocal lattices [41]. [1] During the lattice constant optimizations, all atoms were fixed in the sites of perfect cubic perovskite structure.

The elastic constants are calculated in the standard way [17–19]. The bulk modulus could be calculated in the two ways, firstly as

$$B = \frac{2}{9V_0}\frac{\partial^2 E_{\text{un.cell}}}{\partial V^2}, \tag{3}$$

[1] To achieve high accuracy, large enough tolerances (7, 8, 7, 7, 14) were employed in the evaluation of the overlap for infinite Coulomb and exchange series [18]. In particular, the energy versus strain curves lose their smoothness if smaller tolerances are used. Thus, the truncation parameters have been also selected to reproduce the smooth behavior of the total energy versus the lattice strain.

Table 2
The minimal and maximal exponents of even-tempered Gaussian-type functions (AUX)

	GTF	Min. exponents	Max. exponents
O	s	0.057	200.0
	p	0.07	0.35
	d	0.11	1.6
	f	0.16	0.26
Ti	s	0.2	40.0
	p	0.16	0.5
	d	0.2	1.0
	f	0.3	0.65
Sr	s	0.0585	9.0
	p	0.22	1.0
	d	0.14	0.28
	f	0.3	0.7
Ba	s	0.08	1.2
	p	0.07	1.0
	d	0.08	0.32
	f	0.27	0.3
Pb	s	0.03	0.7
	p	0.07	0.7
	d	0.1	0.12
	f	0.27	0.27

or using the elastic constants [18]:

$$B = (C_{11} + 2C_{12})/3. \tag{4}$$

We present below results for both type of bulk modulus evaluation.

3. Results and discussion

3.1. Bulk properties

To describe three cubic perovskite crystals, we have optimized the lattice constants, independently for the HF and for DFT, separately for each exchange–correlation functional. The results are presented in Table 3. This table allows us to compare our new data with the values obtained previously [16] using the same methods of calculations and the BSs from CRYSTAL's Web-site [26] (results are given in brackets). It is clear from Table 3 that the LDA calculations underestimate the lattice constant for all three perovskites, whereas pure HF and GGA overestimate it as usually. The different GGA schemes give quite good results only for PTO

Table 3
The optimized lattice constant a_0 (Å), bulk modulus B (GPa) and elastic constants C_{ij} (in 10^{11} dyne/cm^2) for three ABO_3 perovskites as calculated using DFT and HF approaches

Method		LDA	PWGGA	PBE	BLYP	P3PW	B3LYP	HF	Experiment	Theory
STO	a_0	3.86 (3.86)	3.95 (3.93)	3.94 (3.93)	3.98 (3.98)	3.90 (3.91)	3.94 (3.94)	3.92 (3.93)	3.89[a] [50] 3.90[b] [49]	3.93 [10] 3.85 [13] 3.86 [8,9] 3.95 [9]
	C_{11}	42.10	31.29	31.93	29.07	31.60	32.83	41.68	31.72[b] [42]	38.9 [8] 30.15 [51]
	C_{12}	12.21	9.80	9.75	9.39	9.27	10.57	7.11	10.25[b] [42]	10.5 [8] 13.74 [51]
	C_{44}	13.32	11.34	11.30	11.09	12.01	12.46	10.50	12.35[b] [42]	15.5 [8] 13.78 [51]
	B	222	170	171	159	167	180	186	174[b] [42]	200 [8] 192 [51]
	B	214 (215)	167 (195)	169 (195)	164 (165)	177 (186)	177 (187)	219 (211)	179 [50] 179 ± 4.6 [52]	203 [13] 204 [9] 167 [9]
BTO	a_0	3.96	4.03	4.03	4.08	4.01	4.04	4.01	4.00 [50]	4.02 [10] 3.94 [8,9] 4.03 [9]
	C_{11}	35.81	30.11	31.04	28.22	31.12	29.75	30.07	20.60 [50] ∼18.70 [43]	35.1 [8]
	C_{12}	11.52	10.35	10.72	10.78	11.87	11.57	13.46	14.00 [50] ∼10.70 [43]	12.5 [8]
	C_{44}	14.98	13.22	13.98	12.24	14.85	14.54	17.34	12.60 [50] ∼11.20 [43]	13.9 [8]
	B	196	169	175	166	183	176	190	162 [50] ∼134 [43]	200 [8]
	B	204	175	180	154	188	172	194	195 ± 5[c] [52] 139[d] [53] 162 [50]	195 [9] 160 [9]
PTO	a_0	3.93	3.96	3.96	4.02	3.93	3.96	3.94	3.97 [54]	3.88 [11] 3.89 [12,8]
	C_{11}	45.03	32.47	34.25	23.03	43.04	34.42	39.83	∼22.90 [43]	32.02 [12] 34.2 [8]
	C_{12}	26.14	15.81	15.52	9.93	24.95	18.08	16.90	∼10.10 [43]	14.12 [12] 14.9 [8]
	C_{44}	11.28	10.69	10.96	8.25	10.93	10.35	17.20	∼10.00 [43]	37.49 [12] 10.3 [8]
	B	324	213	217	143	310	235	245	∼144 [43]	201 [12] 213 [8]
	B	321	246	252	140	279	242	299		203 [12] 209 [8]

The results of previous calculations for non-optimized BS [16] are given in the brackets. Two last columns contain the experimental data and the data calculated using other QM techniques. The penultimate row for each perovskite contains bulk modulus calculated using the standard relation $B = (C_{11} + 2C_{12})/3$, it is done for experiment and theory columns, respectively.

[a] Extrapolated to 0 K.

[b] At room temperature.

[c] Data were taken at phase transition pressure (1.6 GPa).

[d] Data were obtained at room temperature by extrapolation from the high temperature cubic phase above 393 K.

crystal. The PTO lattice constants computed using PWGGA and PBE functionals are close to the experimental values, whereas in other cases the DFT–GGA gives overestimated values. The best

agreement with experimental lattice constant was obtained for the hybrid DFT B3PW and B3LYP methods. On the average, the disagreement between the lattice constants computed using hybrid functionals and experimental values for all three perovskites is less than 0.5%.

Table 3 also lists the computed bulk moduli and the static elastic constants obtained by means of all methods. The presented results for both ways of bulk moduli evaluation differ usually no more than 10–15%. Our calculations confirm the tendency, well known in the literature, that the HF calculations overestimate the elastic constants. The overestimated elastic constants have been indeed obtained here for all three perovskites, when the DFT–LDA scheme was used. In the case of a cubic STO, which is experimentally well investigated, we obtained almost perfect coincidence with the experimental data for both the bulk modulus and elastic constants calculated using B3PW and B3LYP hybrid schemes. The disagreement of elastic constants is less than 5%, and the bulk moduli practically coincide with the experimental magnitudes. The DFT–GGA calculations have tendency to underestimate slightly the bulk modulus, while the lattice constant is overestimated. The elastic constants are underestimated by 5–10% in the GGA calculations. At the same time, the improvement of bulk properties calculated using our newly generated BS, as compared to the old values obtained in our previous computations [14–16] is well seen for STO. In the case of STO, we performed detailed computations previously and a number of detailed experimental data for the STO in cubic phase have been collected by numerous research groups. We would like to stress that the hybrid DFT functionals give the best description of the STO perovskite, i.e. the best agreement with experiment was achieved for both bulk modulus and lattice constant, as well for the elastic constants, and lastly, as will be shown below, for the optical gap as well. Unfortunately, the experimental data for BTO and PTO are more limited. In the case of BTO, relying on the literature data (see Table 3 for references), we chose the DFT B3PW scheme for further calculations, since BTO has the same tendencies as STO in our ab initio calculations. Unlike the cases of BTO and STO, results of computations for PTO perovskite show better agreement with experimental data for DFT B3LYP, PWGGA and PBE. The DFT B3LYP scheme is favored since, as will be shown below, only B3PW and B3LYP give the optical gap close to the experimental one. The last column of Table 3 presents the data of recent QM calculations performed by other theoretical groups (all references are given in Table 3). Most of them have worse agreement with experimental values than our results with the new BSs. Nevertheless, our data correlate well with them, especially with results obtained by King–Smith and Vanderbilt using the DFT–LDA and ultra-soft-pseudopotential augmented-plane-wave method [8]. Furthermore, it is necessary to note that a cubic phase of perovskites is quite unstable, and thus the measured elastic constants strongly depend on the temperature. For example, C_{11} of STO increases by about 4% when the temperature decreases from 30 to −145 °C, as reported by Bell and Rupprecht [42], then C_{11} drops as the phase transition temperature is achieved. The same is true for C_{44} and C_{12}. BTO and PTO elastic constants as a function of temperature are considered in Ref. [43]. Thus, if disagreement for calculated elastic properties with experimental results is about of 10%, it may be considered as a good agreement.

3.2. The electronic properties

All electronic properties have been calculated for the equilibrium geometry for each calculation scheme, respectively. We collected data on the optical gaps in Table 4. Table 5 lists the calculated Mulliken charges and bond populations between an oxygen ion and its neighbors. However, because it is impossible to include so many figures in a paper, in Figs. 2–4 we presented the band structures, the densities of states, and the maps of electron densities for each crystal calculated using the hybrid B3PW functional only.

The band structures of all three perovskites look very similar and agree with band structures published previously in the literature using different ab initio methods and BSs, including plane waves (see, e.g. [9,44]). Nine valence bands derived from O 2p orbitals at the Γ point form the three

Table 4
The calculated optical band gap (eV)

	Optical gap	LDA	PWGGA	PBE	BLYP	P3PW	B3LYP	HF	Experiment
STO	Γ–Γ	2.36	2.31	2.35	2.27	3.96 (4.43)	3.89	12.33	3.75—direct gap
	X–X	2.94	2.79	2.84	2.72	4.53 (5.08)	4.42	13.04	3.25—indirect gap (Ref. [46])
	M–M	4.12	3.69	3.74	3.56	5.70 (6.45)	5.50	14.45	
	R–R	4.77	4.25	4.31	4.09	6.47 (7.18)	6.23	15.72	
	X–Γ	2.78	2.69	2.73	2.63	4.39	4.31	12.86	
	M–Γ	2.15	2.06	2.08	2.03	3.71 (4.23)	3.66	12.02	
	R–Γ	2.04	1.97	1.99	1.94	3.63 (4.16)	3.57	11.97	
BTO	Γ–Γ	1.98	1.97	1.99	1.91	3.55	3.49	11.73	3.2 (Ref. [47])
	X–X	2.85	2.73	2.74	2.57	4.39	4.26	12.83	
	M–M	3.81	3.47	3.50	3.24	5.39	5.19	14.11	
	R–R	4.45	4.03	4.07	3.76	6.12	5.89	15.22	
	X–Γ	2.64	2.55	2.57	2.44	4.20	4.10	12.57	
	M–Γ	2.01	1.93	1.95	1.84	3.60	3.51	11.95	
	R–Γ	1.92	1.84	1.86	1.76	3.50	3.42	11.85	
PTO	Γ–Γ	2.65	2.61	2.65	2.48	4.32	4.15	12.74	3.4 (Ref. [48])
	X–X	1.54	1.68	1.70	1.77	3.02	3.05	10.24	
	M–M	3.78	3.58	3.61	3.33	5.55	5.33	13.76	
	R–R	4.16	3.91	3.94	3.65	5.98	5.78	15.07	
	X–Γ	1.40	1.56	1.58	1.67	2.87	2.92	10.01	
	M–Γ	2.01	1.98	2.00	1.88	3.66	3.53	11.43	
	R–Γ	2.03	1.98	2.00	1.89	3.66	3.52	12.03	

The results of previous CRYSTAL calculations [15] are given in the brackets.

three-fold degenerate levels (Γ_{15}, Γ_{25} and Γ_{15}). The crystalline field and the electrostatic interaction between O 2p orbitals split these bands. But the top of the valence band is displaced from the Γ-point of the Brillouin zone to the R-points in STO and BTO, and to the X-points in PTO. The highest valence electron states at the M point appear only about 0.1 eV below the highest states in R-points, for STO, BTO, and PTO (except HF case). The dispersion of the top valence band is almost flat between R and M points for all three crystals. The highest valence states at the Γ-point stay very close to the top of the valence band in BTO, only 0.1 eV below the R-point. In STO and PTO the difference becomes 0.3 and 0.6 eV respectively. The additional s-orbitals on Pb ions in PTO cause the appearance of an additional valence band below the other bands. They cause also the highest states at the X-point to rise above all other valence states and to make a new top of the valence band. The bottom of the conduction band lies at the Γ-point in all three perovskite crystals. The bottom of the conduction band is presented by the three-fold ($\Gamma_{25'}$) and two-fold (Γ_{12}) degenerate states, which are build from the t_{2g} and e_g states of Ti 3d orbitals, respectively. The electron energy in the lowest conduction band at the X-point is just 0.1–0.2 eV higher than at the bottom of conduction bands. So, there is a little dispersion in the lowest conduction band between the Γ and X points in the Brillouin zone.

The optical band gaps of three perovskites obtained using various functionals are summarized in Table 4. This table clearly demonstrates that pure HF calculations overestimate the optical gap by several times for all three perovskites whereas LDA and GGA calculations dramatically underestimate it. This tendency is well known in solid-state physics. The most realistic band gaps have been obtained using the hybrid B3LYP and B3PW functionals, in agreement with a study by Muscat et al. [45]. These authors show that the hybrid B3LYP functional gives the most accurate estimate of the band gaps in a wide range of materials. The STO experimental band gaps are 3.25 eV (indirect gap) and 3.75 eV (direct gap), as determined by van Benthem et al. using the spectroscopic ellipsometry [46], 3.2 eV band gap has been

Table 5
Effective Mulliken charges, $Q(e)$, and bond populations, P (mili e), for three bulk perovskites, the results of previous calculations [15] are given in brackets

	Atom	Charge Q, bond populations P	LDA	PWGGA	PBE	BLYP	P3PW	B3LYP	HF
STO	Sr^{2+}	Q	1.854 (1.830)	1.853 (1.834)	1.852 (1.832)	1.848 (1.835)	1.871 (1.852)	1.869 (1.852)	1.924 (1.909)
	Ti^{4+}	Q	2.179 (2.126)	2.239 (2.212)	2.245 (2.206)	2.257 (2.266)	2.350 (2.272)	2.369 (2.325)	2.785 (2.584)
	O^{2-}(z)	Q	−1.344 (−1.319)	−1.364 (−1.349)	−1.365 (−1.346)	−1.368 (−1.367)	−1.407 (−1.375)	−1.413 (−1.392)	−1.570 (−1.497)
	O	OI	−52 (−48)	−32 (−34)	−32 (−32)	−30 (−30)	−44 (−36)	−40 (−36)	−58 (−40)
		Sr	−10 (−10)	−6 (−6)	−4 (−6)	−4 (−4)	−10 (−10)	−10 (−8)	−22 (−10)
		Ti	86 (52)	96 (70)	96 (74)	100 (66)	88 (82)	92 (74)	72 (112)
		OII	−8 (−2)	−6 (−2)	−6 (−8)	−6 (−2)	−8 (−4)	−8 (−4)	−12 (−8)
BTO	Ba^{2+}	Q	1.783	1.769	1.766	1.772	1.795	1.796	1.855
	Ti^{4+}	Q	2.195	2.240	2.245	2.252	2.364	2.370	2.808
	O^{2-}(z)	Q	−1.326	−1.337	−1.337	−1.342	−1.386	−1.388	−1.554
	O	OI	−44	−28	−28	−24	−36	−34	−46
		Ba	−34	−26	−24	−22	−34	−32	−52
		Ti	100	104	106	108	100	102	80
		OII	−6	−4	−4	−4	−6	−6	−10
PTO	Pb^{2+}	Q	1.312	1.257	1.231	1.292	1.343	1.407	1.612
	Ti^{4+}	Q	2.172	2.210	2.217	2.232	2.335	2.343	2.785
	O^{2-}(z)	Q	−1.161	−1.156	−1.149	−1.175	−1.226	−1.250	−1.466
	O	OI	−52	−42	−40	−34	−50	−46	−60
		Pb	24	30	32	24	16	14	−20
		Ti	104	108	106	110	98	102	76
		OII	−8	−6	−6	−4	−8	−6	−10

OI means the oxygen nearest to the reference one, OII oxygen from the second sphere of neighbour oxygens. Negative populations mean repulsion between atoms.

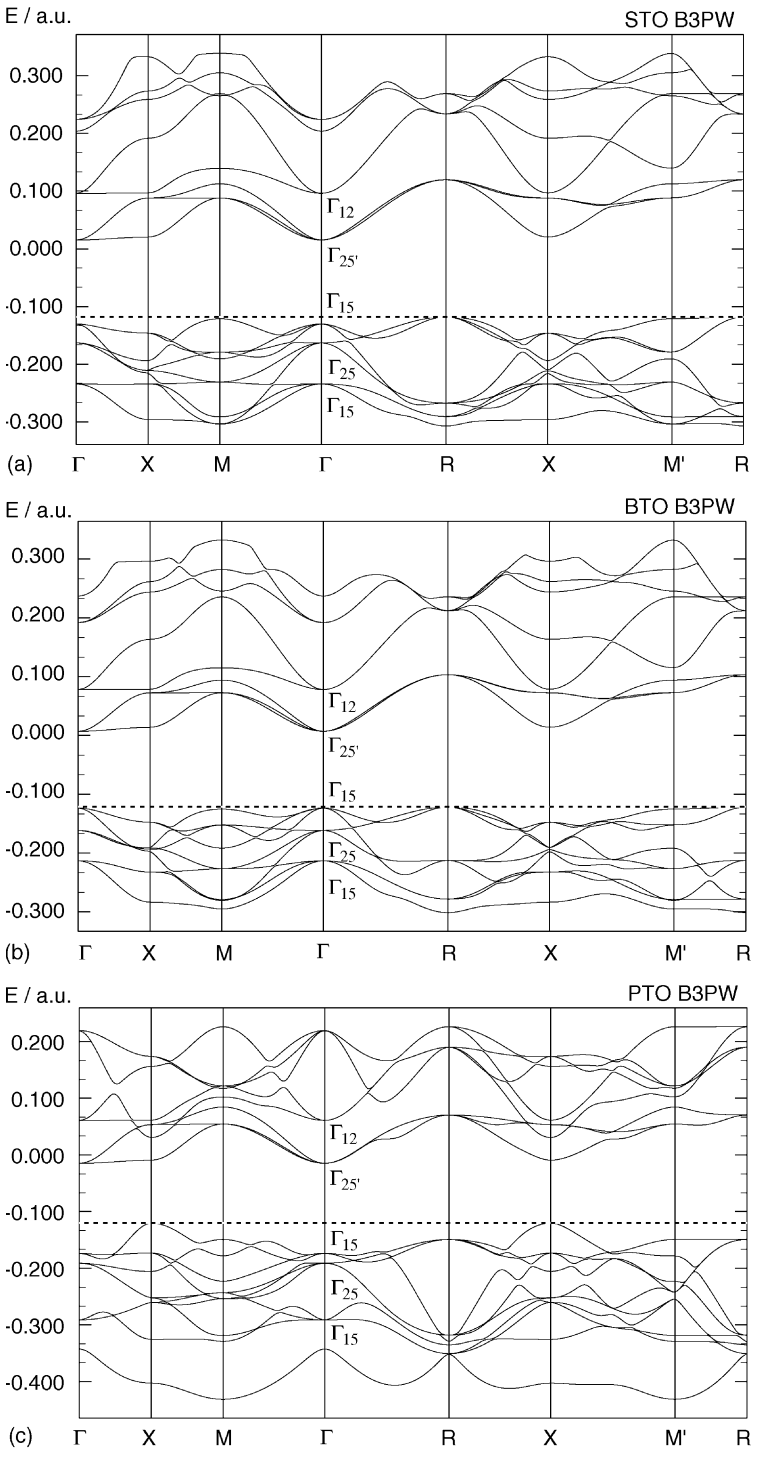

Fig. 2. The band structure of three cubic perovskites for selected high-symmetry directions in the Brillouin zone: (a) STO, (b) BTO, (c) PTO. The energy scale is in atomic units (Hartree), the dashed line is the Fermi level.

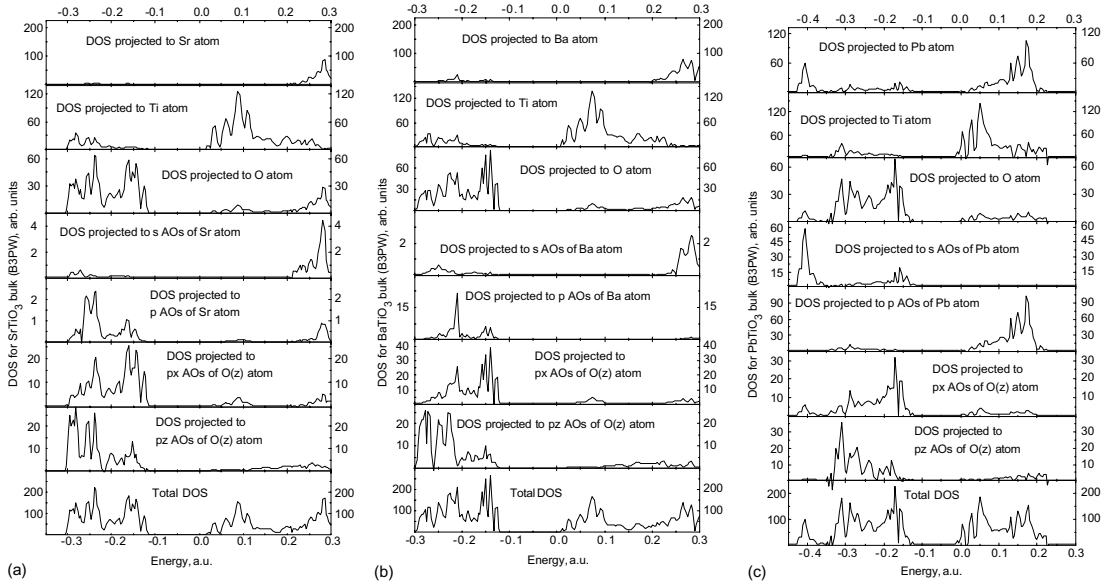

Fig. 3. The calculated total and projected density of states (DOS) for three perovskites: (a) STO, (b) BTO, (c) PTO.

measured for BTO [47] and 3.4 eV for PTO [48]. In our calculations using the B3LYP functional we have obtained the STO indirect band gap (R–Γ) of 3.57 eV to be smaller than 3.89 eV for the direct (Γ–Γ) band gap. Using the B3PW hybrid functional 3.96 and 3.63 eV have been obtained for the STO direct and indirect band gaps, respectively. Our band gaps are very close to the experimental ones. The best agreement with the experimental results (in contrast to our previous calculations given in brackets in Table 4) were obtained due to the adding of d polarization orbital to the basis set of the oxygen atom. The band gaps calculated for BTO and PTO crystals, 3.42 eV and 2.87 eV, respectively, are also in a good agreement with the experiment, the discrepancy is less than 7%. This is acceptable if we take into account difficulties in determining experimentally the band gap, including the optical absorption edge tails which extend up to several tenths of eV [3].

Oxygen p-orbitals give the primary contribution to the valence band of all three studied perovskites. The additional valence band in PTO contains contributions mostly from Pb 6s-orbitals. These orbitals contribute to the valence bands through the entire set of the bands. But these contributions are small, except vicinity of the top of valence spectra. The top of valence bands in STO and BTO is created by O 2p-orbitals, which are perpendicular to the Ti–O–Ti bridge and lie in the SrO– (BaO–) planes. In case of PTO, the top of valence bands contains the same O 2p-orbitals with a significant admixture of Pb 6s-orbitals. The bottom of conduction bands is formed by Ti 3d-orbitals. These orbitals give the main contribution to conduction bands at about the lowest portion (0.1–0.2 atomic units) of the spectrum. There is some small contribution from O 2p-orbitals to this part of the spectrum. Sr(Ba)'s valence s-orbitals and Pb 6p-orbitals contribute to the conduction bands at higher energies. Ti 3d-orbitals also contribute to the lower half of valence state's spectra. Such an admixture of Ti 3d-orbitals to O 2p-orbitals demonstrates of weak covalency of the chemical bonds between Ti and O.

The Mulliken net charges of Ti and O quite differ from the formal ionic charges of ABO_3 perovskites: B^{4+}, and O^{2-}. The reason for this is that, despite the ABO_3 perovskites often are treated as completely ionic, there is a large overlap between the Ti 3d and O 2p orbitals, resulting in a partly covalent O–Ti chemical bonding. This is

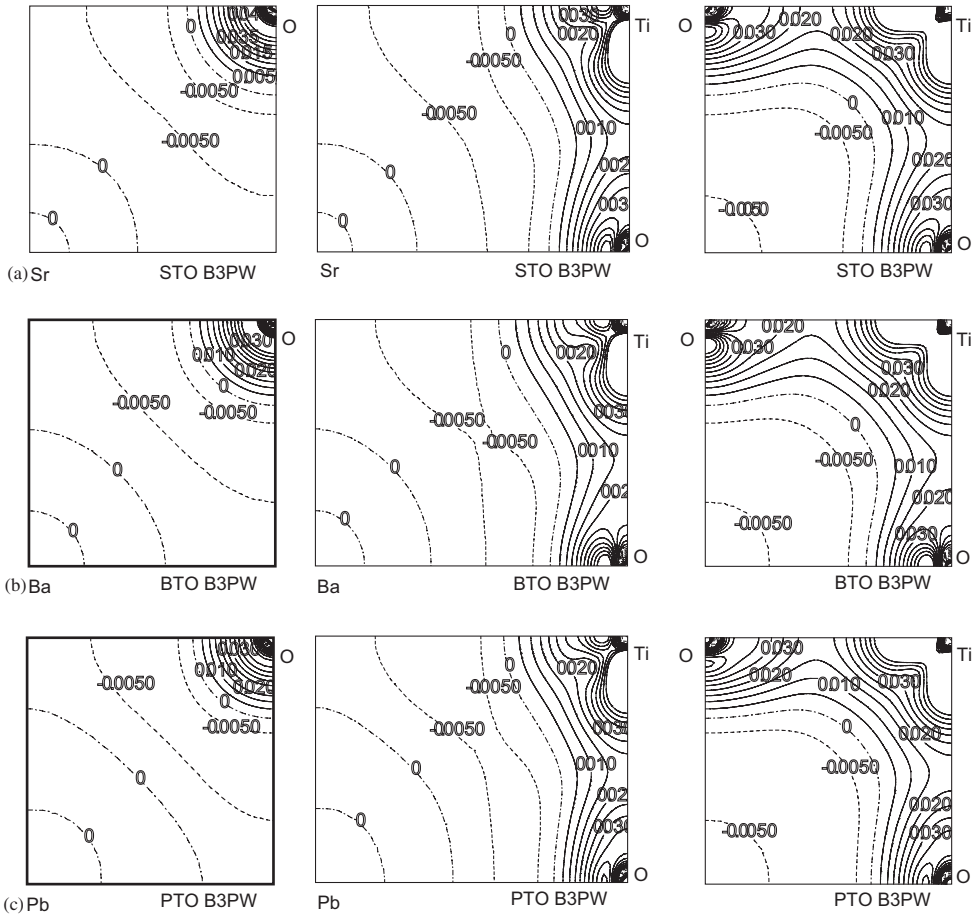

Fig. 4. The difference electron density plots for three perovskites calculated using DFT B3PW: (a) STO, (b) BTO, (c) PTO. The electron density plots are for cross sections shown in Fig. 1a–c. The left column corresponds to Fig. 1a, middle—Fig. 1b, and the right one—Fig. 1c. Isodensity curves are drawn from −0.05 to +0.05 e a.u.$^{-3}$ with an increment of 0.005 e a.u.$^{-3}$.

confirmed by the O–Ti bond populations, which vary from 0.108 to 0.072 e, depending on the calculation method and material. In contrast, there is practically no bonding of O with Sr and Ba atoms in STO and BTO. Sr and Ba charges remain close to the formal +2e. These results are very close for all methods used. The atomic effective charges increase in a series of DFT functionals better accounting for the exchange effect, i.e. LDA, GGA, hybrid functionals, and lastly HF. The calculated optical band gaps (Table 4) also increase in the same series (GGA, LDA, hybrid, HF). Since vacant orbitals in perovskites are localized on cations, an increase of the band gap leads to an additional transfer of the electron density from cations to anions, accompanied by a growth of a crystal ionicity. In contrast, Pb charges turn out to be much less than the formal +2e charge. Also, in contrast to the negative bond populations of STO and BTO, we obtained positive O–Pb bond populations in all DFT calculations, except the HF where it is negative. This means the PTO has a weak covalent O–Pb bonding. The different sign of O–Pb bond population can be explained partly by the fact that "pure" HF calculations do not include the electron correlation corrections. Because a 'large core' ECP was employed for Pb, there was no explicit treatment of 5d orbitals on lead ions. We expect that inclusion of Pb 5d-orbitals could slightly increase the

covalency of the Pb–O bond. The O–O bond populations are always negative. This is evidence that repulsion between oxygens in the perovskites has contributions from both Coulomb interactions, and due to the antibonding interaction.

The difference electron density maps, calculated with respect to the superposition density for A^{2+}, B^{4+}, and O^{2-} ions are presented in Fig. 4. As we mentioned before, we present the electronic density maps obtained only using B3PW hybrid functional. These maps were plotted in the three most significant crystallographic plains, as shown in Fig. 1a–c. Analysis of the electron density maps fully confirms the Ti–O covalent bonding effect discussed above. The positive solid isodensity curves easy distinguishable in Fig. 4 explicitly show the concentration of the electronic density between Ti and O ions. This picture is essentially the same for all three perovskites (see the middle and right columns in Fig. 4, which correspond to the (1 1 0) and TiO_2-(0 0 1) cross sections, respectively). At the same time, the density maps drawn for the AO-(1 0 0) cross section (the left column in Fig. 4) show no trace of the covalent bonding between the oxygen atom and Sr, Ba or Pb. Calculated electron density maps fully confirm the Mulliken population analysis presented in Table 5. The difference electron density maps calculated using X-ray diffraction analysis (see e.g. Ref. [49]) confirm partly covalent nature of the Ti–O bond.

4. Conclusions

We re-optimized in this paper Gaussian-type basis sets for the ab initio simulation of several key perovskite crystals, which permit us to considerably improve quality of calculations of their basic electronic properties based on the HF and DFT SCF LCAO methods combined with six different exchange–correlation functionals. Careful comparison of the seven types of Hamiltonians shows that the best agreement with the experimental results give the hybrid exchange techniques (B3LYP and B3PW). On the other hand, a good agreement between the results computed using the identical Hamiltonians (e.g. LDA), but different type basis sets (e.g. Plane Wave and Gaussian) is observed (see Table 3). Our calculations demonstrate a considerable Ti–O covalent bonding in all three ABO_3 perovskites studied, and an additional weak covalent Pb–O bond in $PbTiO_3$. Results of the present study are used now in our simulations of perovskite surfaces, multi-layered structures, interfaces between perovskites and other materials, and defects in perovskite crystals.

Acknowledgements

This study was partly supported by DFG (SP and RE). Authors are grateful to R. Evarestov, E. Kotomin, and S. Dorfman for fruitful discussions as well as R. Nielson for technical assistance during preparation of the paper.

References

[1] C. Noguera, Physics and Chemistry at Oxide Surfaces, Cambridge University Press, New York, 1996.
[2] V.E. Henrick, P.A. Cox, The Surface Science of Metal Oxides, Cambridge University Press, New York, 1994.
[3] M.E. Lines, A.M. Glass, Principles and Applications of Ferroelectrics and Related Materials, Clarendon Press, Oxford, 1977.
[4] O. Auciello, J.F. Scott, R. Ramesh, Phys. Today 51 (7) (1998) 22.
[5] R.E. Cohen, H. Krakauer, Phys. Rev. B 42 (1990) 6416.
[6] R.E. Cohen, H. Krakauer, Ferroelectrics 136 (1992) 65.
[7] R.E. Cohen, Nature 358 (1992) 136.
[8] R.D. King-Smith, D. Vanderbilt, Phys. Rev. B 49 (1994) 5828.
[9] S. Tinte, M.G. Stachiotti, Phys. Rev. B 58 (1998) 11959.
[10] F. Cora, C.R.A. Catlow, Faraday Discuss. 144 (1999) 421.
[11] P. Ghosez, E. Cockyane, U.V. Waghmare, K.M. Rabe, Phys. Rev. B 60 (1999) 836.
[12] U.V. Waghmare, K.M. Rabe, Phys. Rev. B 55 (1997) 6161.
[13] G. Cappelini, S. Bouette-Russo, B. Amadon, C. Noguera, F. Finocchi, J. Phys.: Condens. Matter 12 (2000) 3671.
[14] S. Piskunov, Y.F. Zhukovskii, E.A. Kotomin, Y.N. Shunin, Comp. Modelling New Technologies 4 (2000) 7–17.
[15] E. Heifets, R.I. Eglitis, E.A. Kotomin, J. Maier, G. Borstel, Surf. Sci. 513 (1) (2002) 211–220.
[16] E. Heifets, R.I. Eglitis, E.A. Kotomin, J. Maier, G. Borstel, Phys. Rev. B 64 (2001) 235417.
[17] C. Pisani (Ed.), Quantum-Mechanical *Ab-initio* Calculations of the Properties of Crystalline Materials, Lecture Notes in Chemistry, vol. 67, Springer, 1996.
[18] V.R. Saunders, R. Dovesi, C. Roetti, M. Causa, N.M. Harrison, R. Orlando, C.M. Zicovich-Wilson,

CRYSTAL'98 User's Manual, Universita di Torino, Torino, 1998.
[19] http://www.chimifm.unito.it/teorica/crystal/crystal.html.
[20] http://www.cse.clrc.ac.uk/cmg/crystal.
[21] M.D. Towler, A. Zupan, M. Causa, Comput. Phys. Commun. 98 (1996) 181.
[22] R. Dovesi, R. Orlando, C. Roetti, C. Pisani, V.R. Saunders, Phys. Status Solidi (b) 217 (2000) 63.
[23] K. Doll, V.R. Saunders, N.M. Harrison, Int. J. Quantum Chem. 82 (2001) 1.
[24] B. Civalleri, P. D'Arco, R. Orlando, V.R. Saunders, R. Dovesi, Chem. Phys. Lett. 348 (2001) 131.
[25] C.M. Zicovich-Wilson, R. Dovesi, V.R. Saunders, J. Chem. Phys. 115 (2001) 9708.
[26] http://www.chimifm.unito.it/teorica/crystal/basis_sets/mendel.html.
[27] P.J. Hay, W.R. Wadt, J. Chem. Phys. 82 (1984) 270.
[28] P.J. Hay, W.R. Wadt, J. Chem. Phys. 82 (1984) 284.
[29] P.J. Hay, W.R. Wadt, J. Chem. Phys. 82 (1984) 299.
[30] W.H. Press, S.A. Teukolsky, W.T. Vetterling, B.P. Flannery, Numerical Recipies in Fortran77, second ed., Cambridge University Press, Cambridge, MA, 1997.
[31] P.A.M. Dirac, Proc. Camb. Phil. Soc. 26 (1930) 376.
[32] S.H. Vosko, L. Wilk, M. Nusair, Can. J. Phys. 58 (1980) 1200.
[33] J.P. Perdew, Y. Wang, Phys. Rev. B 33 (1986) 8800.
[34] J.P. Perdew, Y. Wang, Phys. Rev. B 40 (1989) 3390.
[35] J.P. Perdew, Y. Wang, Phys. Rev. B 45 (1992) 13244.
[36] J.P. Perdew, K. Burke, M. Ernzerhof, Phys. Rev. Lett. 77 (1996) 3865.
[37] A.D. Becke, Phys. Rev. A 38 (1988) 3098.
[38] C. Lee, W. Yang, R.G. Parr, Phys. Rev. B 37 (1988) 785.
[39] A.D. Becke, J. Chem. Phys. 98 (1993) 5648.
[40] H.J. Monkhorst, J.D. Pack, Phys. Rev. B 13 (1976) 5188.
[41] T. Bredow, R.A. Evarestov, K. Jug, Phys. Stat. Sol. (b) 222 (2000) 495.
[42] R.O. Bell, G. Rupprecht, Phys. Rev. 129 (1963) 90.
[43] Z. Li, M. Grimsditch, C.M. Foster, S.K. Chan, J. Phys. Chem. Solids 57 (1996) 1433.
[44] M. Veithen, X. Gonze, P. Ghosez, Phys. Rev. B 66 (2002) 235113.
[45] J. Muscat, A. Wander, N.M. Harrison, Chem. Phys. Lett. 342 (2001) 397.
[46] K. van Benthem, C. Elsasser, R.H. French, J. Appl. Phys. 90 (12) (2001) 6156.
[47] S.H. Wemple, Phys. Rev. B 2 (1970) 2679.
[48] C.H. Peng, J.F. Chang, S. Desu, Mater. Res. Soc. Symp. Proc. 243 (1992) 21.
[49] Y.A. Abramov, V.G. Tsirelson, Acta Cryst. B 51 (1995) 942.
[50] K.H. Hellwege, A.M. Hellwege (Eds.), Ferroelectrics and Related Substances, New Series, vol. 3, Landolt-Bornstein, Springer Verlag, Berlin, 1969, group III.
[51] M.J. Akhtar, Z.N. Akhtar, R.A. Jackson, C.R.A. Catlow, J. Am. Ceram. Soc. 78 (1995) 421.
[52] G.J. Fischer, Z. Wang, S. Karato, Phys. Chem. Minerals 20 (1993) 97.
[53] T. Ishidate, S. Sasaki, Phys. Rev. Lett. 62 (1989) 67.
[54] B.G. Shirane, R. Repinsky, Acta Cryst. 9 (1956) 131.